15th IFK
Proc. of the 15th International Fluid Power Conference <Symposium/Conference>
<DOI>

Geometry-Aware Physics-Informed Neural Network: A Framework for Solving the Reynolds Equation with Starvation for Lubricated Contacts

Faras Brumand-Poor, Artem Konstantinov, Darren Lam Ming Hui, Eric Guntermann, Jakob Wirtz, Katharina Schmitz

RWTH Aachen University, Institute for Fluid Power Drives and Systems (ifas), faras.brumand@ifas.rwth-aachen.de

Abstract.

Machine learning has gained increasing attention in fluid power applications, particularly in condition monitoring and control. A promising development in this field is physics-informed machine learning (PIML), and specifically physics-informed neural networks (PINNs), which integrate governing physical laws directly into the training process. Unlike traditional networks, PINNs do not require data collection and can significantly accelerate computationally demanding simulations. This capability is valuable for studying lubricated contacts, such as seals in pneumatic valves, which operate pneumatic systems by controlling flow rate and pressure, and where accurate yet efficient modeling is essential. Seals are critical for maintaining pressure and preventing leakage; their malfunction can lead to costly failures, downtime, and environmental risks. However, seal behavior remains difficult to characterize due to the coupled hydrodynamic (HD) and elastodynamic (ED) effects within the sealing interface. Conventional elastohydrodynamic lubrication (EHL) simulations based on fluid-structure interaction models provide accurate insights. However, they are computationally expensive, limiting their usability for real-time or large-scale investigations. To address these challenges, this work extends a validated PINN framework for modelling lubrication behavior inside a pneumatic seal by introducing an unsupervised learning autoencoder (AE) to compress complex gap geometries into low-dimensional latent representations. The framework, consisting of a PINN, a loss balancing, and a hyperparameter tuning algorithm, has already been validated for modelling hydrodynamic lubrication simulations with transient phenomena and cavitation. The addition of the AE to the framework yields a geometry-aware PINN (GAPINN) capable of fast, accurate, and geometry-adaptive analysis of sealing systems, thereby enhancing the applicability of PIML in tribological research.

Keywords. Physics-Informed Machine Learning, Hydrodynamic Lubrication, Geometry-Awareness, Autoencoder, Unsupervised Learning, Physics-Informed Neural Networks.

1. INTRODUCTION

Machine Learning has emerged as a promising class of numerous algorithms that can enhance different applications in fluid power, e.g., condition monitoring and control [1, 2].The field of physics-informed machine learning, with its novel class of data-free solvers, the so-called physics-informed neural networks, has shown great potential for accelerating distributed-parameter simulations with the integration of physical laws in the network and without the time-consuming collection of data [3–6]. Accelerating simulation, thus decreasing computational time, is especially relevant for investigating lubricated tribological contacts. One prominent example of such systems is a seal inside a housing and a counter surface, such as a pneumatic valve spool and a lubricant between the seal and the counter surface. Seals are usually less costly than other fluid power components, especially in pneumatic valves, but are crucial for the system. A non-functional seal might result in operational disruptions or a system failure, leading to expensive repairs, delayed production time, and possibly environmental hazards. Seals in fluid power systems are mainly responsible for maintaining operational pressure and preventing leakage. However, the operation of seals generates friction, causing a loss of overall efficiency, especially in pneumatic valves, which exhibit a substantial adverse effect due to increased friction on their dynamic behavior. Despite their significant role in fluid power components and systems, seal behavior is not completely understood due to the complex interactions of hydrodynamic and elastodynamic phenomena [7].

Elastohydrodynamic lubrication simulations or experiments are required to understand these tribological interfaces better. Experiments are rather time-consuming and costly due to the high measurement accuracy needed to obtain valuable information [8]. On the other hand, EHL simulations represent a different approach to obtaining a deeper understanding of these tribological systems by solving the Reynolds equation to compute the hydrodynamic pressure distribution and the deformation within the sealing interface. These EHL simulations primarily consist of a fluid-structure-interaction (FSI), which combines the hydrodynamic pressure buildup of the lubricant with a Finite Element Analysis (FEA) for the deformation. These FSI models provide accurate solutions but exhibit high computational costs [9, 10], which prevents real-time application or a detailed investigation of a significant number of operation points of a sealing system.

These limitations prevent optimal exploitation of sealings for fluid power systems and demand novel approaches for accurate and fast evaluation of different sealing system scenarios. PINNs represent a promising alternative to traditional EHL simulations since they incorporate the same underlying physical equations in the network training process and further solve the investigated scenario in a fraction of the time required by the EHL simulation [11]. Integrating physical laws also dismisses the necessity of data, which is not easily obtained for lubricated contacts, required for regular neural networks.

The first published work applying PINNs to the Reynolds equation was presented by Almqvist in 2021, demonstrating a fundamental implementation of PINNs for this equation [12]. More advanced approaches were later introduced by Zhao et al. and Li et al., who addressed the two-dimensional Reynolds equation for linear sliders and gas bearings, respectively [13, 14]. Rom was the first to develop a PINN capable of solving the stationary Reynolds equation in combination with the Jakobsson–Floberg–Olsson (JFO) cavitation model [15]. Building on this progress, Cheng et al. implemented a PINN framework that

solves the Reynolds equation using either the JFO or the Swift–Stieber (SS) cavitation model, incorporating three different multi-task learning strategies to balance the respective loss terms [16]. Recent work focused on the use of hard constraints to deal with the problem of cavitation [17, 18]. Further research was conducted on the application of hybrid PINNs, combining data-driven approaches and physical laws for the solution of the Reynolds equation [22, 23]. The prior work focused on stationary scenarios; Ramos investigated PINNs for solving the Reynolds equation with time-dependent height changes in journal bearings [25]. Rimon implemented a PINN to solve an elastohydrodynamic lubrication simulation using a simplified stationary one-dimensional Reynolds equation, without cavitation, and incorporating linear pressure-dependent sealing deformation based on the Lamé equation [27]. The mentioned studies focus either on stationary cavitation problems or dynamic problems without cavitation. Furthermore, most developed solutions do not focus on a PINN's ability to understand the investigated geometry. In the work of Rom, the eccentricity of the journal bearing was provided as an input to the PINN, thus adding some geometry-awareness to the PINN. To sum up, the current state of the art in PINNs for modelling hydrodynamic lubrication solves variants of the Reynolds equation; however, there has been little focus on implementing geometry-awareness in PINNs for such applications. The application of geometry-aware PIML has already been successfully used in deformation by implementing geometry-aware PINNs [32, 33] , or directly developing physics-informed graph neural networks (PIGNNs) [34-36].

In this work, a previously validated PINN framework (*ifas HD-Framework*) for seals [3-6] is used. The framework has been applied to solve the Reynolds equation, including transient cavitation modelling, surface roughness, and non-Newtonian lubricant, for interpolation and extrapolation tasks. Interpolation and extrapolation differ in whether the evaluated scenario was included during the training process. The framework has also been applied to solve deformation tasks [34]. The aim of the framework is to eventually model a complete EHL simulation with a PINN-based FSI structure. The hydrodynamic PINN in the framework requires geometric awareness to communicate with the deformation PINN; thus, the framework is extended with an unsupervised learning autoencoder that compresses the high-dimensional gap geometry of a pneumatic seal into a low-dimensional latent vector. This vector is passed to the PINN to create a geometry-aware PINN, which distinguishes itself from the prior framework by enabling the application to different, more complex, and more realistic sealing geometries.

2. HYDRODYNAMIC LUBRICATION – THE REYNOLDS EQUATION WITH CAVITATION MODELING

Elastohydrodynamic lubrication simulations are essential for analyzing wear, friction, and leakage in lubricated mechanical interfaces. These simulations investigate the dynamic interactions between lubricants and contacting surfaces, focusing on the computational modeling of surface deformations and the resulting hydrodynamic pressure within the contact area. They have proved to be pivotal for the design and optimization of tribological contacts across various industrial applications. The DDS (Dynamic Sealing Simulation) model is an advanced simulation framework that has been validated against experimental data under different operating conditions [6]. This model enlightens the complex interactions between a seal and its mating surface, emphasizing the lubricating film that separates them and significantly influences seal behavior. It employs the finite-element software ABAQUS

to simulate seal deformation under various operating conditions accurately, integrating the Reynolds equation through custom user subroutines to calculate hydrodynamic phenomena. This research encompasses the solution of the Reynolds equation as well as the simplification of the model by excluding surface deformation, contact mechanics, and friction. The objective is to study lubrication aspects without the added complexity of deformations. Given its rigorous consistency with experimental results, an accordingly simplified variant of the DDS model will serve as a benchmark for validating the solution of the Reynolds equation in this work.

The Reynolds equation (2.1), as integrated into the DDS model, is based on Osborne Reynolds' original formulation from 1886 and extended by the Jakobsson-Floberg-Olsson cavitation model. It is described as follows [5]:

$$\underbrace{\frac{v}{2}\frac{\partial}{\partial x}((1-\theta)(R_q\Phi^{\tau}+h))}_{Couette\ flow} - \underbrace{\frac{1}{12\eta}\frac{\partial}{\partial x}(\Phi^{p}h^{3}\frac{\partial p}{\partial x})}_{Poiseuille\ flow} + \underbrace{\frac{\partial}{\partial t}((1-\theta)h)}_{Transient\ term} = 0 \tag{2.1}$$

This extension introduces the cavitation fraction concept, represented by the variable θ [8]. The value of θ traditionally denotes the local volume fraction of the gas phase, ranging from zero (no cavitation) to one (complete cavitation). In this work, since a pneumatic system is examined, the cavity fraction is utilized to model the starved film height of the lubricant in the investigated gap, where 0 represents a filled gap and 1 represents an empty gap. The Reynolds equation describes the hydrodynamic pressure p and the cavity fraction (starved lubricant) θ in thin liquid films, accounting for the dynamic viscosity η , the relative velocity v between the contact surfaces, and the gap height h. The variables of time t and position x are also essential to its formulation. Additionally, the model incorporates the shear and pressure flow factors Φ^{τ} and Φ^{p} according to the work of Patir and Cheng [19, 20] allowing for the consideration of surface topography effects on lubrication. Said flow factors are finally complemented by the root mean square roughness R_q, culminating in a partial differential equation that assumes a crucial role in the analysis of lubricated contacts with incompressible fluids.

The Fischer-Burmeister equation (2.2), as employed by Woloszynski et al. [21], establishes the relationship between the p and θ:

$$p + \theta - \sqrt{p^2 + \theta^2} = 0 \tag{2.2}$$

The value of θ provides insight into the occurrence of a starved lubricant within the tribological contact, with the pressure dropping to zero (cf. (2.2)). The JFO cavitation model and its implementation make minimal assumptions about the physical mechanisms leading to a starved lubricant (cavitation), resulting in a non-zero cavity fraction. This allows the model to track lubricant distribution in tribological contacts with limited lubricant supply, such as grease-lubricated sealing contacts in pneumatic spool valves. In these cases, a non-zero cavity fraction indicates partial filling of the sealing gap. Both the Reynolds and the Fischer-Burmeister Equations are structured to equate to zero, establishing the groundwork for the computation of physics-based losses for neural networks, as will be demonstrated during this paper.

3. MATERIALS AND METHODS

3.1. *Hydrodynamic Lubrication and the Potential of Physics-Informed Neural Networks*

As introduced in Chapter 2, one essential mathematical tool for simulating the pressure distribution in lubricated contacts is the Reynolds equation. Numerical techniques like finite volumes, finite elements, or finite differences are usually used to solve tribological issues in situations like the Reynolds equation, where an analytical solution is not available. However, using numerical approaches frequently necessitates a significant amount of computing power and has proven to be very time-intensive. The solution may lie in the realms of PIML, which has recently shown considerable promise in tribology, facilitating notable advancements [10, 24].

To improve the depiction of phenomena like wear, lubrication, and friction, PIML, more specifically PINNs, incorporates models with physical principles to direct the learning process, in contrast to typical machine learning techniques that only use data-driven methodologies [10, 26]. PINNs employ a neural network for predictive purposes but are trained with applicable laws of physics by including residual terms derived from PDEs in the loss function [28]. Therefore, these models frequently produce results that are more accurate and reliable than those obtained using only data-driven approaches and are used in a variety of tribological applications, ranging from the anticipation of wear or damage to the assessment of lubrication conditions on hydrodynamic surfaces.

Like conventional neural networks, PINNs process inputs like position x, time t, and further case-dependent parameters. The network's output is produced after these input values are processed by the network's hidden layers that comprise a predefined number of neurons. Each neuron carries out a series of mathematical operations that culminate in a complex function, which is then characterized as the network's output.

Once the network has produced an output, the training commences, involving the computation of various supervised and unsupervised losses that are then utilized in the enhancement of neuron parameters, namely the weight and bias.

Figure 3.1 illustrates an exemplary PINN. The network depicted is a hybrid PINN consisting of three physics-informed and one data-driven components. The available data is employed to accelerate the convergence of the governing equations, thereby facilitating the attainment of a more accurate solution.

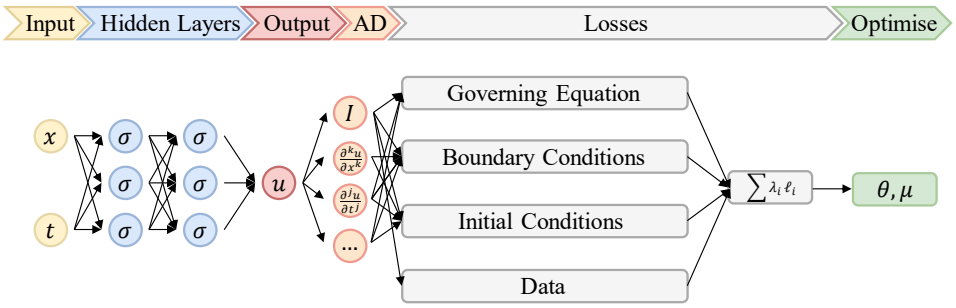

Figure 3.1: Schematic illustration of a PINN [3]

The residual loss (or Governing Equations-Loss, as depicted in Figure 3.1) coincides with the residuals of the governing physical equations, making this an unsupervised loss since there is no direct comparison to a reference value [29]. The evaluation of the loss is conducted at designated spatial and temporal locations, referred to as collocation points, by inserting the PINN's outputs at said points into the governing physical equations and determining the residuals. At this point, it becomes apparent why equations (2.1) and (2.2) must equate to zero (as mentioned in Chapter 2), because the residual between the PINN's output and the governing equations at specific collocation points can only be computed if the right side equals zero.

In addition to the residual losses, PINNs also rely on losses associated with boundary and initial conditions. The objective of said losses is to guarantee that the prescribed boundary and initial conditions for the partial differential equation are satisfied. The presence of a direct value comparison in this loss computation makes these two losses subject to supervisory control. The data loss term corresponds to the classical data-driven loss. Following the determination of the individual losses, the loss terms are then each multiplied by a weight factor and added together. Subsequently, the network parameters $\vec{\theta}$ are optimized so that the weighted loss sum is minimized.

3.2. The ifas HD-Framework

Having established the fundamental principles of hydrodynamic lubrication and the use of PINNs in this realm, the following section will present the structure of the ifas HD-Framework. For a more detailed description also regarding the parameter of the framework and the whole training process the reader is advised to refer to this work [3]. The ifas HD-Framework comprises three main pillars that are all implemented in the Python programming language: the HD-PINN, the Bayesian Optimizer from the Keras Tuner Library [30] and the Adaptive Moment Estimation Optimizer from the Keras Library [31].

The training in this framework begins by employing the Bayesian Optimizer to find the optimal hyperparameters (HP) for the HD-PINN. These include all the parameters that are necessary for the initial construction of the PINN. After that, the PINN computes the initial pressure and cavity fraction distribution for the given input and initializes the loss functions. The iterative body of the training process involves adapting the network parameters $\vec{\theta}$ by the Adam Optimizer based on the loss functions and a consequential recalculation of the pressure and cavitation distribution by the PINN. Once the desired number of epochs has been achieved, the training has completed, and the PINN's losses are transferred back to the Bayesian Optimizer to complete the final optimization of the hyperparameters for that training.

Contrary to previous studies, the HD-PINN in this work consists of a PINN that is preceded by an autoencoder. Figure 3.2 illustrates the novel hydrodynamic framework with the AE, which processes the sealing and counter surface's high-dimensional height profile, provided by the finite-element software ABAQUS, through a Python interface with the encoder to a low-dimensional latent vector consisting of n_{latent} height parameters. To validate the compression, the decoder reconstructs the latent space into a high-dimensional height profile, which is then compared to the original profile. Subsequently, the latent vector

$$\vec{h}_{latent} := \left[h_1, h_2, \dots, h_{n_{latent}}\right] \tag{3.1}$$

is passed to the hydrodynamic PINN in an input vector $\vec{\mathcal{P}}$

$$\vec{\mathcal{P}} := \left[\vec{x}, t, p_l, p_r, \theta_l, \theta_r, \rho, \eta, R_q, \Phi^\tau, \Phi^p, v, h_{lubricant}, \vec{h}_{latent}\right] \text{ with} \tag{3.2}$$

$$\vec{x} := [x_1, x_2, \dots, x_{200}] \tag{3.3}$$

which is then presented to each neuron of the first hidden layer.

Within each of the $n_{neurons}$ neurons in the n_{layers} hidden layers of the PINN, the respective inputs of a single neuron are multiplied by a weight w, summed up, and finally offset with the bias b of the current neuron.

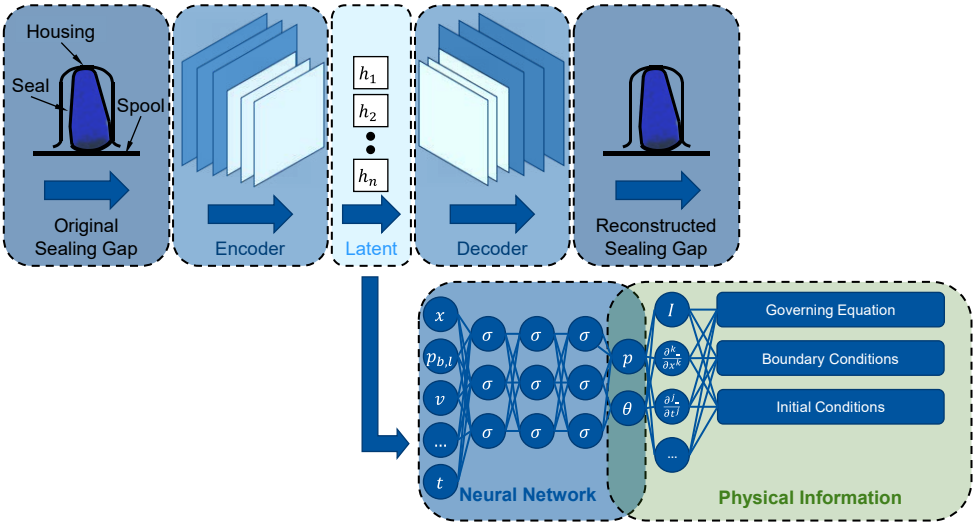

Figure 3.2: The ifas HD-GAPINN

The result will then serve as the input of the neuron's activation function f whose evaluation is then characterized as the neuron's output σ. These individual outputs are required for the solution of the governing equations, namely the Reynolds and Fischer-Burmeister equations, as well as the boundary and initial conditions. In this work, the layer size $n_{neurons}$ will stay constant across all n_{layers}. Additionally, all neurons in one layer will host the same activation function f, thus a different activation function can only be achieved in a different layer. Eventually, the PINN computes the pressure p and the cavity fraction θ, depending on the network parameters $\vec{\Theta}$:

Once the PINN has produced its output, various losses are calculated to ensure its accuracy. These losses include a residual loss for both the Reynolds- and Fisher-Burmeister equation (domain Ω), a boundary condition loss (domain Γ) and an initial condition loss (domain Υ). Partial derivations that may occur in the complex differential equations during loss computation ($\frac{\partial^k u}{\partial x^k}, \frac{\partial^j u}{\partial t^j}, \dots$), are usually determined by employing automatic differentiation (AD), which efficiently computes gradients of any order with machine accuracy by applying differential rules such as the chain and product rule. However, in all its efficiency, the computation of partial derivatives with AD relies on the prerequisite of a continuous function. It thus introduces a limitation into loss calculations, as it does not adequately

account for inputs of a discrete nature. When aiming for a high degree of realism in the underlying simulation, the processing of discrete inputs becomes indispensable because realistic geometries are captured through discrete measurements into a height profile. Thus, to address this limitation, this work will use the finite-difference method (FDM), more specifically, the central finite-difference scheme, for the computation of partial derivatives.

4. RESULTS

Having outlined the methodology used to achieve the research objectives of this work in the previous section, this section presents the obtained results. The results of this study encompass a variation of two geometries ("*Slight Seal Contact*" and "*Seal Geometry with Kinks*") across two different scenarios, namely both with and without the consideration of cavitation modelling. In each test case ("*Slight Seal Contact*", "*Seal Geometry with Kinks*"), the autoencoder was trained with latent-space sizes of 8, 16, and 32, leading to height latent vectors of the exact dimensions that were consequently provided to the PINN.

4.1. Slight Seal Contact without Cavitation Modelling

This first presented test case is characterized by a slightly stressed seal with a force exerted on the housing and prolonged onto the seal. Since cavitation is not taken into consideration, the loss calculation for this test case solely revolves around the residual and pressure boundary condition loss $\mathcal{L}_{\Omega_{Residual}}$ and $\mathcal{L}_{\Gamma_p}$. This specific test case is relevant for assessing the accuracy of the PINN's geometry-aware loss computation, which relies on finite difference schemes to approximate the derivatives of the height profile. Figure 4.1 shows the results of the AE with different latent size (8, 16, 32), the results of the PINN and the relative error of the PINN ($p_{PINN} - p_{DDS}/p_{DDS}$). For each latent size, the reconstruction of the height and the pressure computation of the PINN yield good results. In Figure 4.1 (left column), the PINN configured with an 8-dimensional latent space shows a maximum absolute percentage pressure error of 1.4%. By expanding the latent representation to 16 dimensions, the peak absolute percentage discrepancy decreases to 1.2%, indicating a slight improvement in accuracy. Further increase of the latent size to 32 yields a maximum absolute percentage error of around 1.5%, thus worse than the smaller latent sizes. An increase in the latent size does not necessarily result in a better performance of the PINN. The latent size primarily affects the performance of the compression and reconstruction of the AE. Since all three variants show a good match between the original and reconstructed height profiles, the use of a smaller latent size allows for the possibility of using a smaller network size, as the layer sizes should be proportional to the number of inputs. Thus, the size of the latent space should be selected rather smaller and can be checked by the reconstruction accuracy of the AE. The increase in latent size does not necessarily translate into better physical fidelity and may, in fact, introduce unnecessary complexity that hinders generalization. Overparameterization can lead to overfitting or suboptimal convergence, especially when the problem geometry does not warrant such a high-capacity representation.

In summary, this test case demonstrates that increasing the latent dimension from 8 to 16 improves the quality of the predicted pressure field by enabling the PINN to better resolve small variations in geometry. However, further increase to 32 dimensions offers no clear advantage and slightly worsens performance, emphasizing the importance of balancing representational power with the complexity of the underlying physical domain.

Nevertheless, each investigated latent size shows good results in combination with the PINN.

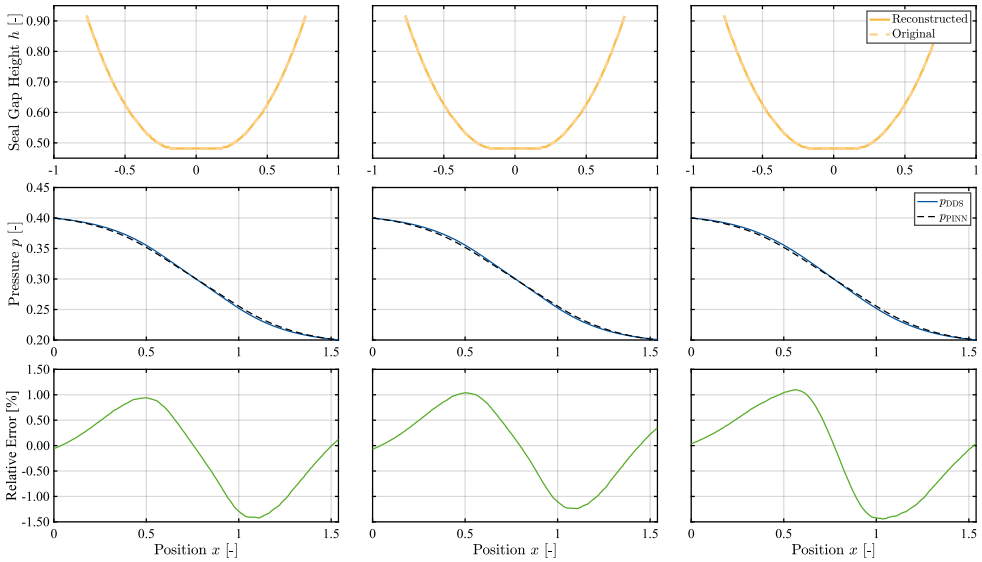

Figure 4.1: Pressure Distribution for Geometry "*Slight Seal Contact*"

4.2. Seal Geometry with Kinks without Cavitation Modelling

This second investigated test case is characterized by a seal that is pressed against a diagonal slider and thus contains kinks and steep gradients. Analogously to the test case "*Slight Seal Contact*" without the consideration of starved film height, the loss calculation for this test case revolves around the residual and pressure boundary condition loss $\mathcal{L}_{\Omega_{Residual}}$ and $\mathcal{L}_{\Gamma_p}$.

This test case was designed to evaluate the PINN's capabilities in handling high height gradients, which is particularly relevant for this geometry-aware PINN because its loss computation relies on a finite-difference scheme for the derivatives of the height profile. Finite-difference schemes, being numerical, introduce an error into the computation that can severely alter the result if said computation proves to be vulnerable to error propagation. This is especially the case when error-prone intermediate results experience a potentiation. According to Equation (2.1), such a potentiation of the height profile in combination with its x-derivative is introduced in the Reynolds equation and thus also in the computation of the Reynolds loss term (scaled with the factor three, cf. x-derivation of h^3 in Reynolds equation (2.1)).

The results shown in Figure 4.2 demonstrate a slightly worse approximation of the pressure distribution for lower latent space sizes than the previous test cases; the maximum absolute percentage error reaches up to 2% for latent space sizes of 8 and 16. For the 32-LS case, however, the PINN manages to obtain excellent results, leaving the maximum absolute percentage deviation from the ifas DDS-reference below 0.7%.

Clearly, the PINN profited from a higher resolution of the challenging height profile. This may be attributed to a better performance of the finite-difference Method for higher latent space sizes, resulting in a more accurate loss computation and thus a more effective training.

Nevertheless, the performance in all three test cases is sufficient for a precise modelling of the hydrodynamic pressure.

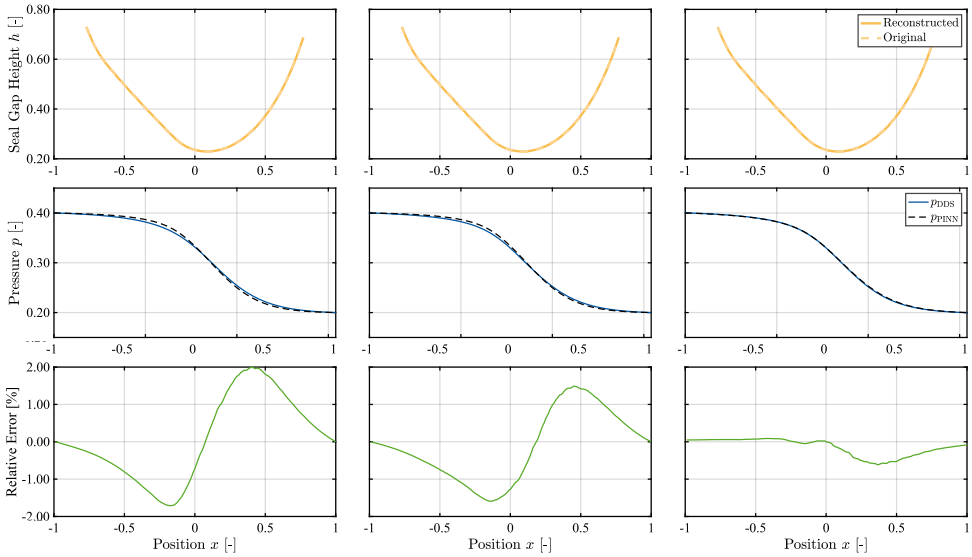

Figure 4.2: Pressure Distribution for Geometry "*Seal Geometry with Kinks*"

4.3. Slight Seal Contact with Cavitation Modeling

The following section extends the first test case by including the starved film height, which increases the complexity of the PINN's training. In contrast to the previous test cases, the PINN's training now incorporates all losses described in Section 3.2. In addition, a Filtered Absolute Error metric is used to compare the results between the PINN and the DDS for the cavity fraction and pressure. This accounts for differences in numerical precision between the two methods. For instance, in regions where cavitation should ideally be zero, the DDS may yield values on the order of 10^{-20}, while the PINN may only approximate this with values around 10^{-5}. The usage of a relative error in these areas would not adequately illustrate the accuracy of the PINN. By using the "Rolling Mean" filter, the mentioned outliers from the absolute error $|(p,\theta)_{PINN} - (p,\theta)_{DDS}|$ are eliminated.

In this test case, shown in Figure 4.3, the PINN does not perfectly reproduce the pressure and cavitation peaks. However, for the 16-LS and 32-LS cases, the pressure peaks are well captured, with absolute errors of less than 0.05. The sharp cavitation peak remains a challenge across all latent space sizes, with maximum absolute errors ranging between 0.01 to 0.15. It becomes apparent that the inclusion of cavitation significantly increases the complexity of the problem, making it more challenging for the PINN to correctly identify the regions of maximum pressure and cavitation. Nonetheless, the performance of the PINN could potentially be improved through extended Bayesian Optimization training, allowing for the discovery of more optimal hyperparameters and a better global minimum.

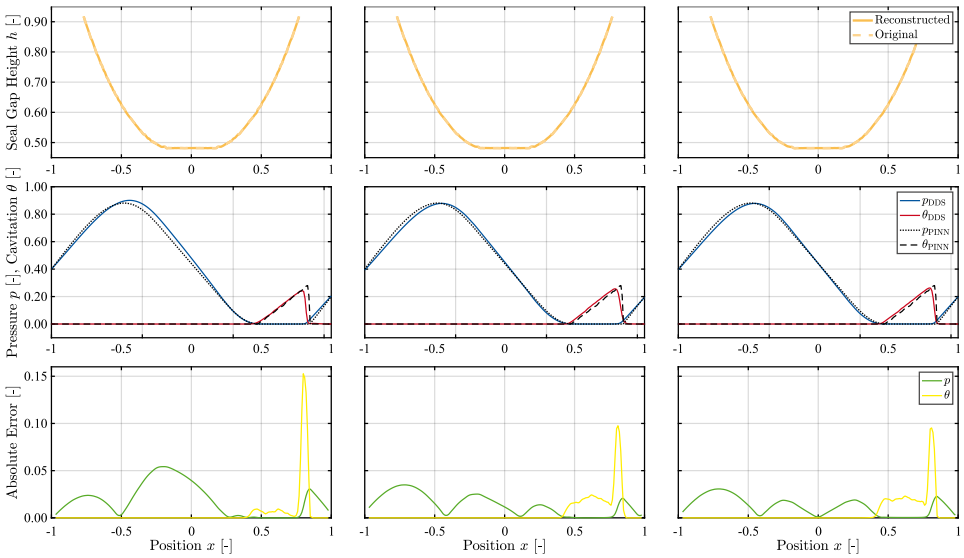

Figure 4.3: Pressure and Cavitation Distribution for Geometry "*Slight Seal Contact*"

It is worth noting that the application of soft-constraints is not expected to improve the overall results. This is because soft-constraints primarily assist in the transition regions between pressure and cavitation, rather than directly enhancing the PINN's ability to identify the locations of maximum pressure and cavitation. Therefore, they do not offer a complete solution for addressing the PINN's limitations in capturing these critical features. Nevertheless, all three setups display good agreement between the PINN and the numerical solver, especially when considering the speedup from four milliseconds to one to two seconds (Intel I9 13th-generation processor, 128 GB RAM DDR5, and Nvidia RXT 4090) in terms of computation time for PINN and DDS. Table 4.1 summarizes the results of the different test case by displaying the mean absolute error (MAE) and the root mean squared error (RMSE) and underline the high accuracy for each test case and each latent size.

Case	**Latent**	**MAE p**	**MAE θ**	**RMSE p**	**RMSE θ**
1	32	0.0050	-	0.0060	-
1	16	0.0024	-	0.0029	-
1	8	0.0027	-	0.0033	-
2	32	0.0020	-	0.0018	-
2	16	0.0027	-	0.0020	-
2	8	0.0028	-	0.0021	-
3	32	0.0118	0.0056	0.0151	0.0205
3	16	0.0134	0.0057	0.0172	0.0193
3	8	0.0185	0.0057	0.0254	0.0279

Table 4.1: Mean absolute error and root mean squared error for each test case

To sum up, the results show that the extension of the AE enables the PINN to obtain geometry-awareness and solve each test case with high accuracy for all three latent sizes. Since all latent sizes displays sufficient accuracy, the usage of a smaller latent size is promising since it would less increase the input size of the PINN and thus keep the whole framework as lightweight as possible.

5. CONCLUSION

This work focused on the conception, implementation, and testing of a geometry-aware physics-informed neural network, comprising the HD-PINN from the ifas HD-Framework and an extension that enables it to process more complex and realistic geometries. The extension included the finite-element software ABAQUS for the seal model, a Python interface that extracted height profiles from ABAQUS, and an autoencoder that enabled the compression of those height profiles to make the input processable for the PINN. The PINN's capabilities in the pressure and cavitation prediction for lubricated sealing gaps in pneumatic valves were then assessed in three test scenarios. All pressure and cavitation distributions produced by the PINN were then systematically compared to those generated by the ifas DDS for the identical test scenarios.

This work represents the next step in implementing a PINN-based fluid-structure interaction for elastohydrodynamic lubrication simulations. The novel framework extends the current state-of-the-art of PINNs in hydrodynamic lubrication by adding geometry-awareness and enables the coupling with the deformation part of the elastohydrodynamic simulation. Furthermore, the findings show that the PINN can process a latent representation of a high-dimensional variable, which is a promising result, since the PINN for the deformation also needs to process the high-dimensional load, described by the hydrodynamic pressure vector, coupled in the fluid-structure-interaction. To sum up, the findings underline the potential of PINNs to model elastohydrodynamic behavior in lubricated contacts in pneumatic seals, and the next steps are to implement an AE for the deformation PINN and, eventually, couple all components in a fluid-structure-interaction.

6. ACKNOWLEDGEMENTS

The authors thank the Research Association for Fluid Power of the German Engineering Federation VDMA for its financial support (grant: FKM No. 7058400). Special gratitude is expressed to the participating companies and their representatives in the accompanying industrial committee for their advisory and technical support.

7. REFERENCES

[1] Brumand-Poor, F., Makansi, F. et al. 'Implementation of Variational Autoencoder for Dimension Reduction of a Hydraulic System', 2022 Global Fluid Power Society Ph.D. Symposium, 2024. DOI: 10.13052/rp-9788770047975.

[2] Brumand-Poor, F., Kauderer, L. et al. 'Application of Deep Reinforcement Learning Control of an Inverted Hydraulic Pendulum', International Journal of Fluid Power, 2023. DOI: 10.13052/ijfp1439-9776.2429.

[3] Brumand-Poor, F., Bauer, N. et al. 'FAST COMPUTATION OF LUBRICATED CONTACTS: A PHYSICS- INFORMED DEEP LEARNING APPROACH', 14th International Fluid Power Conference, pp. 254–266, 2024. DOI: 10.13052/rp-9788770042222C19.

[4] Brumand-Poor, F., Barlog, F. et al. 'Advancing Lubrication Calculation: A Physics-Informed Neural Network Framework for Transient Effects and Cavitation Phenomena in Reciprocating Seals', 22nd International Sealing Conference 2024, 2024. DOI: 10.61319/J7I2HNKR.

[5] Brumand-Poor, F., Rom, M. et al. 'Physics-Informed Deep Learning for Lubricated Contacts with Surface Roughness as Parameter', Tribologie und Schmierungstechnik, Vol. 71, Nr. 4, 2024. DOI: 10.24053/TuS-2024-0021.

[6] Brumand-Poor, F., Azanledji, F. K. et al. 'Extrapolation of cavitation and hydrodynamic pressure in lubricated contacts: a physics-informed neural network approach', Advanced Modeling and Simulation in Engineering Sciences, Vol. 12, Nr. 1, 2025. DOI: 10.1186/s40323-025-00283-9.

[7] Bauer, N., Baumann, M. et al. 'Elastohydrodynamic Simulation of Pneumatic Sealing Friction Considering 3D Surface Topography', Chemical Engineering & Technology, Vol. 46, Nr. 1, pp. 167–174, 2023. DOI: 10.1002/ceat.202200471.

[8] Wohlers, A., Heipl, O. et al. 'Numerical and Experimental Investigation on O-Ring-Seals in Dynamic Applications', International Journal of Fluid Power, Vol. 10, Nr. 3, pp. 51–59, 2009. DOI: 10.1080/14399776.2009.10780988.

[9] Dakov, N. 'Elastohydrodynamische Simulation von Wellendichtungen am Beispiel der PTFE-Manschettendichtung mit Rückförderstrukturen', Universität Stuttgart, 2020. DOI: 10.18419/opus-10997.

[10] Marian, M., Tremmel, S. 'Current Trends and Applications of Machine Learning in Tribology—A Review', Lubricants, Vol. 9, Nr. 9, pp. 86, 2021. DOI: 10.3390/lubricants9090086.

[11] Marian, M., Tremmel, S. 'Physics-Informed Machine Learning--An Emerging Trend in Tribology', Lubricants, Vol. 11, Nr. 11, pp. 463, 2023. DOI: 10.3390/lubricants11110463.

[12] Almqvist, A. 'Fundamentals of Physics-Informed Neural Networks Applied to Solve the Reynolds Boundary Value Problem', Lubricants, Vol. 9, Nr. 8, pp. 82, 2021. DOI: 10.3390/lubricants9080082.

[13] Li, L., Li, Y. et al. 'ReF-nets: Physics-informed neural network for Reynolds equation of gas bearing', Computer Methods in Applied Mechanics and Engineering, Vol. 391, pp. 114524, 2022. DOI: 10.1016/j.cma.2021.114524.

[14] Zhao, Y., Guo, L., Wong, P. P. L. 'Application of physics-informed neural network in the analysis of hydrodynamic lubrication', Friction, Vol. 11, Nr. 7, pp. 1253–1264, 2023. DOI: 10.1007/s40544-022-0658-x.

[15] Rom, M. 'Physics-informed neural networks for the Reynolds equation with cavitation modeling', Tribology International, Vol. 179, pp. 108141, 2023. DOI: 10.1016/j.triboint.2022.108141.

[16] Cheng, Y., He, Q. et al. 'HL-nets: Physics-informed neural networks for hydrodynamic lubrication with cavitation', Tribology International, Vol. 188, pp. 108871, 2023. DOI: 10.1016/j.triboint.2023.108871.

[17] Xi, Y., Sun, R. 'Inverse problems in hydrodynamics lubrication: Parameter identification in the Reynold equation by using physics-informed neural networks', Proceedings of the Institution of Mechanical Engineers, Part J: Journal of Engineering Tribology, Vol. 239, Nr. 4, pp. 423–435, 2025. DOI: 10.1177/13506501241291403.

[18] Xi, Y., Deng, J., Li, Y. 'A new method to solve the Reynolds equation including mass-conserving cavitation by physics informed neural networks (PINNs) with both soft and hard constraints', Friction, 2024. DOI: 10.1007/s40544-023-0791-1.

[19] Patir, N., Cheng, H. S. 'An Average Flow Model for Determining Effects of Three-Dimensional Roughness on Partial Hydrodynamic Lubrication', Journal of Lubrication Technology, Vol. 100, Nr. 1, pp. 12–17, 1978. DOI: 10.1115/1.3453103.

[20] Patir, N., Cheng, H. S. 'Application of Average Flow Model to Lubrication Between Rough Sliding Surfaces', Journal of Lubrication Technology, Vol. 101, Nr. 2, pp. 220–229, 1979. DOI: 10.1115/1.3453329.

[21] Woloszynski, T., Podsiadlo, P., Stachowiak, G. W. 'Efficient Solution to the Cavitation Problem in Hydrodynamic Lubrication', Tribology Letters, Vol. 58, Nr. 1, 2015. DOI: 10.1007/s11249-015-0487-4.

[22] Zhao, Y., Wong, P. P. L. 'A hybrid data-driven approach for the analysis of hydrodynamic lubrication', Proceedings of the Institution of Mechanical Engineers, Part J: Journal of Engineering Tribology, Vol. 238, Nr. 3, pp. 320–331, 2024. DOI: 10.1177/13506501231214584.

[23] Shutin, D., Kazakov, Y. et al. 'Data-driven and physics-informed approaches for improving the performance of dynamic models of fluid film bearings', Tribology International, Vol. 191, pp. 109136, 2024. DOI: 10.1016/j.triboint.2023.109136.

[24] Paturi, U. M. R., Palakurthy, S. T., Reddy, N. S. 'The Role of Machine Learning in Tribology: A Systematic Review', Archives of Computational Methods in Engineering, Vol. 30, Nr. 2, pp. 1345–1397, 2023. DOI: 10.1007/s11831-022-09841-5.

[25] Ramos, D. J., Cunha, B. Z., Daniel, G. B. 'Evaluation of physics-informed neural networks (PINN) in the solution of the Reynolds equation', Journal of the Brazilian Society of Mechanical Sciences and Engineering, Vol. 45, Nr. 11, 2023. DOI: 10.1007/s40430-023-04418-0.

[26] Raissi, M., Perdikaris, P., Karniadakis, G. E. 'Physics-informed neural networks: A deep learning framework for solving forward and inverse problems involving

nonlinear partial differential equations', Journal of Computational Physics, Vol. 378, pp. 686–707, 2019. DOI: 10.1016/j.jcp.2018.10.045.

[27] Rimon, M. T. I., Hassan, M. F. et al. 'A Design Study of an Elasto-Hydrodynamic Seal for sCO2 Power Cycle by Using Physics Informed Neural Network', ASME Power Applied R&D 2023, 2023. DOI: 10.1115/POWER2023-108802.

[28] Nabian, M. A., Meidani, H. 'Physics-Driven Regularization of Deep Neural Networks for Enhanced Engineering Design and Analysis', Journal of Computing and Information Science in Engineering, Vol. 20, Nr. 1, 2020. DOI: 10.1115/1.4044507.

[29] Cai, S., Mao, Z. et al. 'Physics-informed neural networks (PINNs) for fluid mechanics: a review', Acta Mechanica Sinica, Vol. 37, Nr. 12, pp. 1727–1738, 2021. DOI: 10.1007/s10409-021-01148-1.

[30] O'Malley, Tom and Bursztein, et. al. 'KerasTuner', https://github.com/keras-team/keras-tuner, 2019.

[31] Chollet, F. e. a. 'Keras', https://github.com/fchollet/keras, 2015.

[32] Oldenburg, J., Borowski, F. et al. 'Geometry aware physics informed neural network surrogate for solving Navier–Stokes equation (GAPINN)', Advanced Modeling and Simulation in Engineering Sciences, Vol. 9, Nr. 1, 2022. DOI: 10.1186/s40323-022-00221-z.

[33] Nguyen, T. N. K., Dairay, T. et al. 'Geometry-aware framework for deep energy method: an application to structural mechanics with hyperelastic materials', http://arxiv.org/pdf/2405.03427v1, 2024.

[34] Brumand-Poor, F., Trautmann, M., Schmitz, K. 'Advancing deformation calculation: a physics-informed deep graph learning framework for hyperelastic materials', Advanced Modeling and Simulation in Engineering Sciences, Vol. 12, Nr. 1, 2025. DOI: 10.1186/s40323-025-00304-7.

[35] Scarselli, F., Gori, M. et al. 'The graph neural network model', IEEE Transactions on Neural Networks, Vol. 20, Nr. 1, pp. 61–80, 2009. DOI: 10.1109/TNN.2008.2005605.

[36] Dalton, D., Husmeier, D., Gao, H. 'Physics-informed graph neural network emulation of soft-tissue mechanics', Computer Methods in Applied Mechanics and Engineering, Vol. 417, pp. 116351, 2023. DOI: 10.1016/j.cma.2023.116351.

Biographies

Faras Brumand-Poor received a bachelor's degree in electrical engineering from RWTH Aachen University in 2017, a master's degree in electrical engineering from RWTH Aachen University in 2019, and a master's degree in automation engineering from RWTH Aachen University in 2020, respectively. He is the Group Leader of the research groups Fluids and Smart Systems and the Deputy Chief Engineer at the Institute for Fluid Power Drives and Systems at RWTH Aachen University. His research areas include machine learning, particularly deep learning, physics-based learning, fluid transmission lines, and virtual sensory systems.

Prof. Katharina Schmitz studied mechanical and chemical engineering at RWTH Aachen University and Carnegie Mellon University, Pittsburgh (USA) and graduated 2015 as Dr.-Ing. at RWTH Aachen University. Since 2018, she is full professor at RWTH Aachen University and director of the Institute for Fluid Power Drives and Systems (ifas). In addition, she is Vice Dean of the Faculty for Mechanical Engineering at RWTH Aachen, a position she holds since 2020. Prof. Schmitz’s awards and honors include several best paper awards and 2023 IMechE Joseph Bramah Medal award.